IOP Publishing Journal of Physics: Condensed Matter
J. Phys.: Condens. Matter **32** (2020) 175702 (10pp) https://doi.org/10.1088/1361-648X/ab6a2f

Theoretical study of oxygen insertion and diffusivity in the γ-TiAl $L1_0$ system

Damien Connétable[1], Aurélien Prillieux[1], Camille Thenot[2] and Jean-Philippe Monchoux[2]

[1] CIRIMAT, UMR 5085, CNRS INP UPS, ENSIACET 4, allée Émile Monso, BP 44362, F-31030 Toulouse Cedex 4, France
[2] CEMES CNRS UPR 8011, 29 Rue Jeanne Marvig, F-31055 Toulouse, France

E-mail: damien.connetable@ensiacet.fr

Received 19 September 2019, revised 9 December 2019
Accepted for publication 10 January 2020
Published 28 January 2020

Abstract

This work is a first-principles study of the insertion and diffusivity of oxygen in the γ-TiAl $L1_0$ system. Five interstitial positions were identified as stable. One, however, the *2h* site a pyramid composed of a Ti square topped by an Al atom, was found more stable than the others. The oxygen interactions with the TiAl system were thus studied and analyzed in detail using vibrational, elastic and electronic properties. The results show that the O atom prefers to be surrounded by Ti atoms and tries to minimize the number of bonds with aluminum. The diffusion mechanism is subsequently studied at the atomic scale, by analyzing displacements between stable interstitial sites. The oxygen diffusivity is found to be anisotropic and the components in the x and z direction, D_x and D_z, are then calculated and compared with those of O diffusion into other Ti–Al alloys. The analysis of results shows two effects. First, the stability of sites is related to the number of O–Al bonds, the fewer there are, the more stable the site is, and second, the diffusion is faster when the content of interstitial sites composed of many Ti atoms is low.

Keywords: TiAl, oxygen, solubility, diffusivity, first-principles calculations

(Some figures may appear in colour only in the online journal)

1. Introduction

Intermetallic TiAl-based alloys are promising materials for aircraft engines due to their high specific properties as compared to Ni-based superalloys [1–3]. However, Ti–Al-based alloys react with the environment thereby leading to oxidation [4, 5] and embrittlement [6] phenomenon. In both cases, the bulk diffusion of oxygen in Ti–Al-based alloys is involved but this has surprisingly not been deeply investigated. Moreover, several studies showed that in these alloys, oxygen interacts with dislocations and may be responsible for fine precipitation [7] resulting in a change in the mechanical properties of the alloy [8, 9]. Ti–Al alloys are mainly composed of two phases: γ-TiAl and α_2-Ti_3Al. A few studies showed that the oxygen solubility in the γ-TiAl is around 250 at.ppm [10]. However, the oxygen solubility strongly depends on γ phase composition and temperature. Several authors reported that oxygen solubility increased when the aluminum content of the gamma phase decreased [9, 10]. On the other hand, there is no data in the literature about the oxygen diffusion in γ-TiAl. Further, knowledge of the oxygen diffusion would be extremely useful to understand the preferential internal oxidation of the γ phase in α_2-Ti_3Al + γ-TiAl alloys [4].

In this study, the effects of interface segregation (i.e. TiAl–Ti_3Al, grain-boundaries) and the formation of clusters, as mentioned in the case of bcc-Fe [11] or fcc-Ni [12] were neglected in first-approximation. Indeed, these could modify the solubility and the diffusion process and solubility. The aim of the present work is therefore to analyze the insertion and diffusivity of O atoms in the γ-TiAl system, and to propose a diffusion coefficient that can be compared with that of other Ti–Al systems.

The article is organized as follows. Section 2 summarizes the method and calculations details. In section 3, O insertion in the TiAl system is investigated and the interactions between oxygen and the network are described and analyzed. Section 4 subsequently discusses the diffusion mechanisms.

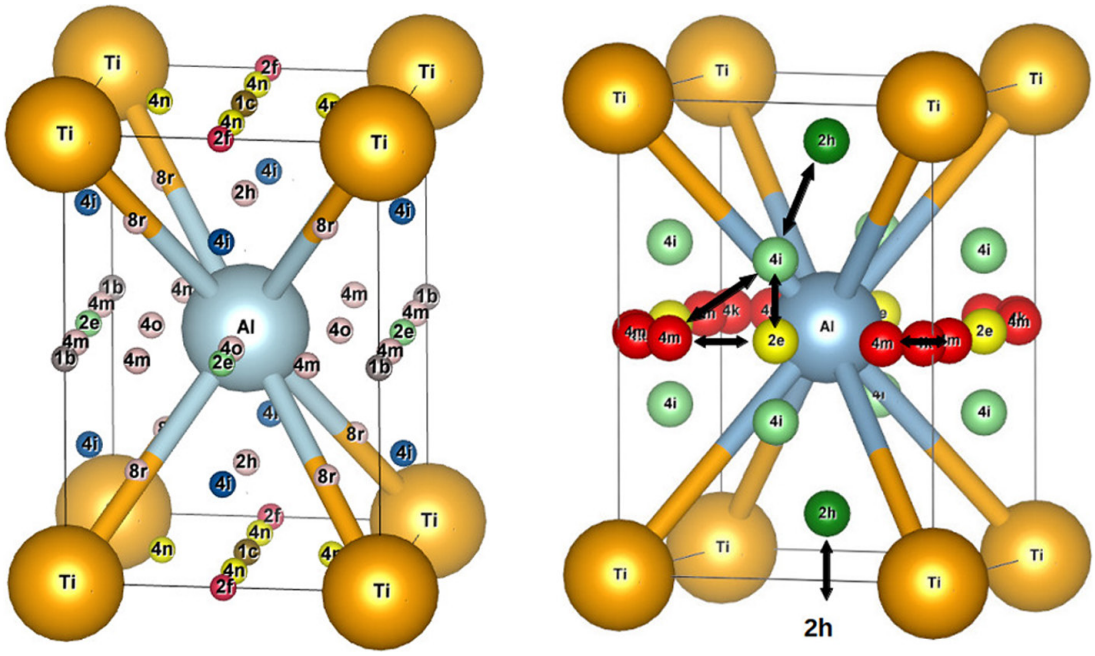

Figure 1. Schematic representations of the TiAl- $L1_0$ structure (bold-centered tetragonal representation) indicating the interstitial positions tested (left), and the stable positions (right).

2. Methodology

To study the insertion of O atoms in the TiAl system, DFT calculations were performed using the Vienna *ab initio* Simulation Package (VASP) [13]. The self-consistent Kohn–Sham equations were solved using the projector augmented wave (PAW) pseudo-potentials method [14] and with the Perdew–Burke–Ernzerhof generalized gradient approximation of the exchange and correlation functional (PBE) [15]. The investigations showed that TiAl is non-magnetic, wether with or without O insertion. Calculations were thus performed without magnetism. A kinetic energy cut-off of 600 eV was used for the plane-wave basis set. Γ-centered $20 \times 20 \times 20$ Monkhorst–Pack **k**-meshes [16] were used to sample the first Brillouin zone of the primitive cell. For large super-cells, the band-folding method was used to reduce the **k**-points meshes. The forces and the stress tensor were relaxed and calculations were performed at zero pressure.

The investigation of migration processes at the atomic scale was conducted through NEB calculations on $3 \times 3 \times 3$ super-cells [17]. Five intermediate positions were used for each 'trajectory'. The energy of the transition states was then calculated using the same criteria of convergence as for insertion sites. In the Eyring transition state theory [18], the key quantity at the atomic scale is the probability of leaving a site a to a site b. This probability is given by the jump rate, Γ_{ab}, computed by:

$$\Gamma_{ab}[T] = \frac{k_B T}{h} \frac{\mathcal{Z}_{TS}}{\mathcal{Z}_a} \exp\left[-\frac{\Delta E_m^{ab}}{k_B T}\right] \tag{1}$$

where ΔE_m^{ab} is to the migration energy to go from a to b, $\mathcal{Z}_{TS}$ the (vibration) partition function for the transition state and $\mathcal{Z}_a$ the (vibration) partition function for the initial state, i.e. a. $\mathcal{Z}$ is linked to the Helmholtz free energies, F_v, by

$$F_v = -k_B T \ln \mathcal{Z} \tag{2}$$

where F_v is given by:

$$F_v = k_B T \sum_{\nu=1}^{3N} \int n_\nu(\mathbf{q}) \ln\left[2 \sinh\left(\frac{\hbar \omega_{\nu,\mathbf{q}}}{2 k_B T}\right)\right] \mathrm{d}\mathbf{q} \tag{3}$$

$\omega_{\nu,\mathbf{q}}$ are the frequencies in the wave vector $\mathbf{q}$ and the mode ν. Vibrational properties were performed on $3 \times 3 \times 3$ super-cells, i.e. 54 atoms, for each configuration (insertion sites and transition states). Phonon free energies were therefore calculated to analyze configuration stability and to compute $\mathcal{Z}$. The summation was done on fine $\mathbf{q}$-mesh grids (i.e. $20 \times 20 \times 20$). This was done by using the *phonopy* package [19].

3. Insertion of oxygen in the TiAl system

The γ-TiAl $L1_0$ structure belongs to space group *123* (P4/mmm, *tP2*). It is a tetragonal structure, where Ti and Al atoms occupy *1a* and *1d* positions, respectively. The $L1_0$ structure can be depicted as an ordered centered-tetragonal structure where the two types of atoms alternate in the (0 0 2) atomic planes. In this representation, the lattice parameters a_o and c_o are equal to 3.999 and 4.076 Å respectively. To simplify, a bct representation was used Ti atoms occupying the corners of the tetragonal lattice and Al atom the center. The lattice parameters are thus equal to 2.822 and 4.074 Å, see figure 1. As shown by Connétable [20], interstitial species can then occupy various sites in the $L1_0$ system, as represented in figure 1. Eleven Wyckoff positions were tested: *1b*, *1c*, *2e*, *2f*, *2h*, *4i*, *4k*, *4m*, *4n*, *4o* and *8r* positions. Atomic positions are given in table 1.

In the TiAl- $L1_0$ structure, there are four non-equivalent octahedral sites: *1c*, *2e*, *1b* and *2f* sites. *1c* and *2e* sites (resp.

Table 1. Wyckoff positions and site symmetry extracted from [21].

1b	*1c*	*2e*	*2f*
(0, 0, 1/2)	(1/2, 1/2, 0)	(0, 1/2, 1/2) (1/2, 0, 1/2)	(0, 1/2, 0) (1/2, 0, 0)
2h	*4i*	*4m*	*4n*
(1/2, 1/2, -z_h) (1/2, 1/2, z_h)	(0, 1/2, z_i) (1/2, 0, z_i) (0, 1/2, -z_i) (1/2, 0, -z_i)	(x_m, 0, 1/2) (−x_m, 0, 1/2) (0, x_m, 1/2) (0, −x_m, 1/2)	(x_n, 1/2, 0) (−x_n, 1/2, 0) (1/2, x_n, 0) (1/2, −x_n, 0)
4k	*4o*	*8r*	
(x_k, x_k, 1/2) (−x_k, −x_k, 1/2) (−x_k, x_k, 1/2) (x_k, −x_k, 1/2)	(x_o, 1/2, 1/2) (−x_o, 1/2, 1/2) (1/2, x_o, 1/2) (1/2, −x_o, 1/2)	(x_r, x_r, z_r) (−x_r, x_r, z_r) (−x_r, x_r, -z_r) (x_r, x_r, -z_r)	(−x_r, −x_r, z_r) (x_r, −x_r, z_r) (x_r, −x_r, -z_r) (−x_r, −x_r, -z_r)

Table 2. Insertion energies (E_i, in eV), zero-point energies (ZPE, in meV) and enthalpy energies (H_f, in eV) of an oxygen atom in different configurations. The zero point energy of the O_2 molecule is equal to 45 meV. ΔH is the energy difference (in eV) between the *2h* site and the other sites.

	nb atom	*1b*	*1c*	*2e*	*2f*	*2h*	*4i*	*4k*	*4m*
		Unstable	Unstable	—	Unstable	$z_h = 0.109$	$z_i = 0.330$	$x_k \simeq$ 0.044	$x_m = 0.234$
E_i	16	−2.369	−3.366	−2.921	−0.421	−3.368	−2.555	−2.365	−2.369
	54	−2.310	−3.393	−2.522	−0.341	−3.460	−2.571	−2.317	−2.319
	128	−2.344	-3.443	−2.589	−0.529	−3.484	−2.601	−2.349	−2.347
ZPE		—	—	−5	—	13	7	−20	−10
H_f		—	—	−2.594	—	−3.471	−2.594	−2.369	−2.357
ΔH		—	—	0.88	—	0	0.88	1.10	1.11

1b and *2f* sites) correspond to two non-equivalent octahedral sites where interstitial atoms are surrounded by four Ti (resp. Al) atoms and two Al (resp. Ti) atoms. Each octahedral configuration differs from the others in the distance between first-nearest neighboring atoms, Al–Al, Ti–Al and Ti–Ti. In addition, the *4i*, *4n* and *4m* positions correspond to three non-equivalent tetrahedral sites. As for the bcc structures, the volume defined by the tetrahedral site is inside the octahedral volume.

Simulations were conducted on three different sizes of super-cell: $2 \times 2 \times 2$ (16 atoms), $3 \times 3 \times 3$ (54 atoms) and $4 \times 4 \times 4$ (128 atoms) super-cells. Larger super-cells were considered large enough to accurately compute the insertion energy in the limit of infinite dilution. However, for numerical reasons, using intermediate size super-cells, $3 \times 3 \times 3$, is a good compromise. They were hence used to compute phonon properties and study migration processes. The insertion energy of an O atom in an interstitial site, E_i, is expressed by:

$$E_i = E_o[\mathrm{TiAl} + \mathrm{O}] - E_o[\mathrm{TiAl}] - \frac{1}{2}E_o[\mathrm{O_2}] \qquad (4)$$

where E_o energies correspond to the DFT energies. The reference state for oxygen is the O_2 molecule. $E_o[O_2]$ was computed with the spin effects. E_i values are listed in table 2 for stable configurations only.

After relaxation, eight configurations remain stable: *1b*, *1c*, *2e*, *2f*, *2h*, *4i*, *4k* and *4m*. Two of them, *2h* and *1c*, have almost the same lowest energy, about −3.48 eV. From a geometrical point-of-view, both configurations are very similar. The analysis of phonons nevertheless shows that the *1c* site is not a local minimum, as shown in figure 2. When the O atom moves slightly away from the *1c* site, it always falls into one of the two neighboring *2h* sites. It is a 'stable' configuration for symmetry reasons only (by symmetry, forces along the *c* axis are equal to zero). Therefore, the only stable position, *2h*, is located near the top face of the unit-cell, about 0.4 Å up/down of the [0 0 1] face, as displayed in figure 1. The Al–O distance is then equal to 1.85 Å, and to 2.08 Å for Ti–O. The other configurations are found almost 900 meV higher in energy than *2h*, see table 2. Moreover, *4i* and *2e* (resp. *4k* and *4m*) configurations almost have the same energy, about −2.6 eV (resp. −2.4 eV). Regarding these sites, positions are also rather near, $d(4i - 2e) \simeq 0.7$ Å, see figure 1. Phonon calculations show that they are all stable, as discussed below. This result is unusual because, there are three stable near-neighboring sites in the *x* (resp. *z*) direction. Finally, as regards *1b* ($\Delta H = 0.940$ eV) and *2f* ($\Delta H = 2.955$ eV) sites, their insertion energy is high in comparison with *2h* sites.

Configuration stability was analyzed by studying interatomic force constants (IFC). Results (phonon density-of-states only) are displayed in figures 2 and 3, for unstable and stable configurations, respectively. Three configurations, *1b*, *1c* and *2f*, show imaginary (negative here) frequencies associated with the O atom, see figure 2. These positions are thus unstable. The analysis of vibrations shows that there are two imaginary frequencies in the case of *1b* and *2f* but only one in

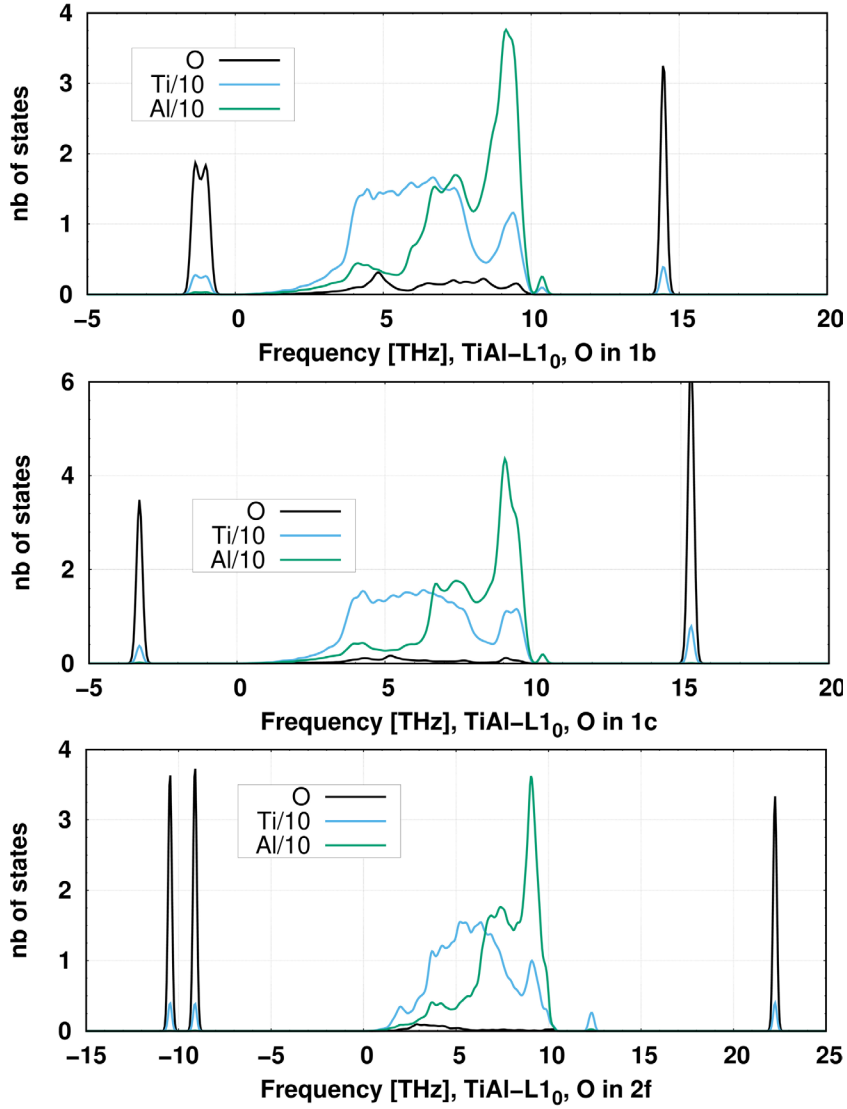

Figure 2. Projected density-of-states (pDOS) of O in *1b*, *1c* and *2f* sites (from top to bottom). The amplitude of the pDOS onto Ti and Al atoms was divided by 10. Frequencies are expressed in THz.

the case of *1c*. When the O atom is located in the *1c* site, it is located in the transition state between two first nearest-neighboring *2h* positions, as explained above. For the *1b* and *2f* configurations, many 'equivalent' stable positions are located around these positions. In such sites, the O atom could move into one of the four neighboring stable sites. This explains the two imaginary frequencies. These are second-order transition states, as mentioned in [22]. Concerning stable sites, in the *4k* case, there is a peak around 1THz mainly associated with the O atom (in addition to the high frequencies associated with O atoms, too). This result suggests that this site must be located in the vicinity of a transition state. It can also be noticed that the pDOS of the *4m* and *4k* sites are strongly similar, except that the low-energy peak in the *4k* pDOS is split into two small peaks and that O frequencies are shifted at higher energies. For the other stable sites, the vibrations of the O atom are decoupled from the rest of the network. It is in the *2h* sites that the O atom least modifies the phonon of the bulk. Finally, there are five stable positions for the O atom in the TiAl system: *2e*, *2h*, *4i*, *4k* and *4m*, as displayed in figure 3.

The zero-point energies (ZPE), H_v, were afterwards computed with the following expression:

$$H_v = F_v[\mathrm{TiAl} + \mathrm{O}] - F_v[\mathrm{TiAl}] - \frac{1}{2}F_v[\mathrm{O_2}], \qquad (5)$$

where F_v is the Helmholtz free energy given by the equation (3). Values are reported in table 2. The zero-point energy is found low, <20 meV, as compared to hydrogen [20]. The *2h* and *4i* configurations have the same enthalpy energy.

These results can now be compared with literature values. Bakulin *et al* [23] also studied oxygen solubility in the TiAl system using first-principles calculations. However, they only considered five sites in their paper, labeled O1, O2, O3, O4 and T. Here is the site notation equivalence: O1 = *1c*, O2 = *1b*, O3 = *2e*, O4 = *2f* and T = *4i*. The *2h* site was not taken into account, nor were the *4m* and *4n* sites. By analyzing their NEB calculations (see figure 1, [23]), a minimum can be identified in the path along O1-T, which should be the *2h* site. Bakulin *et al* explain that the O atom should occupy the O1 (*1c*) site and that the *1b* and *2f* sites are stable. This is in contradiction with the

present phonon results. However, from an energy standpoint, the insertion energy of their configurations are in agreement with our results. Wei *et al* [24] briefly studied the insertion of oxygen into octahedral/tetrahedral sites. They gave energies for two 'octahedral sites', −4.20 and −3.20 eV, which should correspond to *1c* and *1b* sites (or maybe the *2e* and *2f* sites).

In terms of experimental values, there is no solubility energy in the literature. The direct comparison with theoretical and experimental values is therefore difficult. Only some values of the amount of oxygen dissolved in Ti–Al alloys was reported in the literature. A qualitative discussion can thus be proposed based on these results. Menand *et al* [10] showed that the oxygen concentration in the TiAl system, about 100–250 appm, is lower than in the Ti_3Al- $D0_{19}$ system, >1000 appm. Theoretical results show the same tendency: the values of oxygen insertion energy in the γ-TiAl system, $\simeq$-3.5 eV, is higher than in the α_2-Ti_3Al system, −6.2 eV [23–25]. Menand provided an explanation as to why O solubility is lower in TiAl than in Ti_3Al. He argued that 'the presence of cavities surrounded by Ti atoms only are supposed to be convenient for interstitials'. DFT results clearly confirm this hypothesis: Bakulin [25] showed that the octahedron *2a* site (space group 194) surrounded by Ti atoms only is the most stable site in the Ti_3Al system, and our results show that in the TiAl system, the *2h* site in the most stable. However, contrary to the assumption of Menand, the preferred site is neither an octahedral nor a tetrahedral site, but the *2h* site, which is a pyramid formed by 4 Ti atoms and one Al atom. In this position, the O atom thus limits the number of first nearest neighboring Al atoms (just one) and optimizes the number and length of its Ti bonds (four). In comparison with other possible configurations, like *2c* or *4o* sites for instance, Ti–O bonds are the shortest in *2h*.

To quantify precisely the interaction between the O atom and the TiAl metal, elastic (elastic dipoles, relaxation volumes, etc) and electronic (Bader charges, charge transfer) properties were investigated. Data are listed in table 3.

Elastic dipole tensors, $\mathcal{P}_{ij}$, and the relaxation volume, Ω_r, were calculated by using the method of Varvenne *et al* [26]. Values given in table 3 were obtained for $3\times3\times3$ super-cells. $\mathcal{P}_{ij}$ quantify rather precisely the elastic effects induced by the insertion of an atom or a defect on a crystal. Conversely, they also are a good means to quantify the effect of stresses applied to the system on the behavior of interstitials. Due to the symmetry break, when oxygen occupies an interstitial site, the components of the elastic tensors differ greatly on the crystallographic direction. For instance, in the case of the *2c* site, the diagonal elements are equal to 9.2 and −2.8 eV. The positive (resp. negative) sign along one direction means that the inserted atom tends to dilate (resp. contract) the material in this direction. The least anisotropic tensor is associated with the most stable site, i.e. the *2h* site, which corresponds to a minimum elastic distortion of TiAl. Ω_r values predicted by elastic theory are moreover in excellent agreement with DFT calculations of the formation volume $\Omega_f = V[\mathrm{TiAl+O}] - V[\mathrm{TiAl}]$ (where V is the volume of the super-cell with and without oxygen). The distortion of the crystal due to the insertion of oxygen is important, about 10 $\mathring{A}^3$, as compared to the case of hydrogen, about 2 $\mathring{A}^3$ [20].

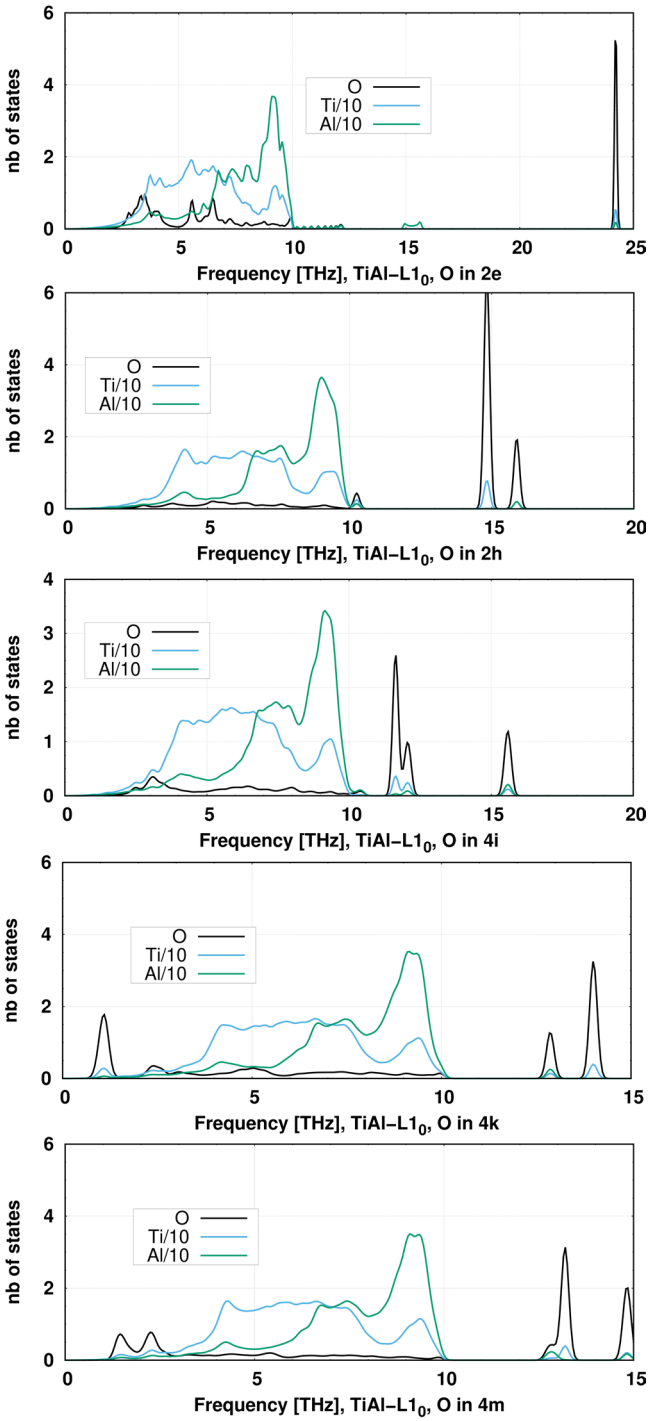

Figure 3. From top to bottom, pDOS of O in the *2e*, *2h*, *4i*, *4k* or *4m* sites.

From an electronic standpoint, when an O atom occupies an interstitial site, the charge transfer calculated by using the Bader charge [27], $\mathcal{B}$, is found high, about 1.7*e*, regardless of the site considered. The main contribution to the charge transfer comes thus from 1NN Al atoms. Therefore, the O atoms interact mainly with Al atoms, which induces modifications of the Ti–Al bonds. To confirm this, the charge transfers, $\Delta\rho = \rho[\mathrm{TiAl+O}] - \rho[\mathrm{TiAl}] - \rho[\mathrm{O}]$, were drawn in figure 4.

Table 3. Calculated values of the Bader charge ($\mathcal{B}$, in e^-) of O, Al and Ti (both in first-nearest neighboring position of oxygen) atoms, the volume of formation (Ω_f, in $\mathring{A}^3$), the volume of relaxation (Ω_r) and the elastic dipoles ($\mathcal{P}_{ij}$, in eV). The number of electrons of each specie used in the pseudo-potential (labeled †) is given as well as the Bader charge of Al and Ti in TiAl- $L1_0$ (labeled ‡).

			2e	*2h*	*4i*	*4k*	*4m*
$\mathcal{B}$	O	(6†)	7.7	7.6	7.6	7.8	7.7
	Al	(3†, 3.7‡)	3.1	3.0	3.0	3.2	3.1
	Ti	(10†, 9.3‡)	9.3	9.2	9.1	9.3	9.2
Ω_f			7.0	6.4	10.7	5.9	7.6
Ω_r			7.8	6.3	10.8	5.7	6.4
$\mathcal{P}_{ij}$			$\begin{bmatrix} 9.8 & 6.5 & 0 \\ 6.5 & 9.8 & 0 \\ 0 & 0 & -2.8 \end{bmatrix}$	$\begin{bmatrix} 4.3 & 0 & 0 \\ 0 & 4.3 & 0 \\ 0 & 0 & 4.8 \end{bmatrix}$	$\begin{bmatrix} 9.1 & -1.6 & 0 \\ -1.6 & 9.1 & 0 \\ 0 & 0 & 5.0 \end{bmatrix}$	$\begin{bmatrix} 4.2 & 0 & 0 \\ 0 & 2.2 & 0 \\ 0 & 0 & 5.7 \end{bmatrix}$	$\begin{bmatrix} 4.1 & 0.6 & 0 \\ 0.6 & 4.1 & 0 \\ 0 & 0 & 5.5 \end{bmatrix}$

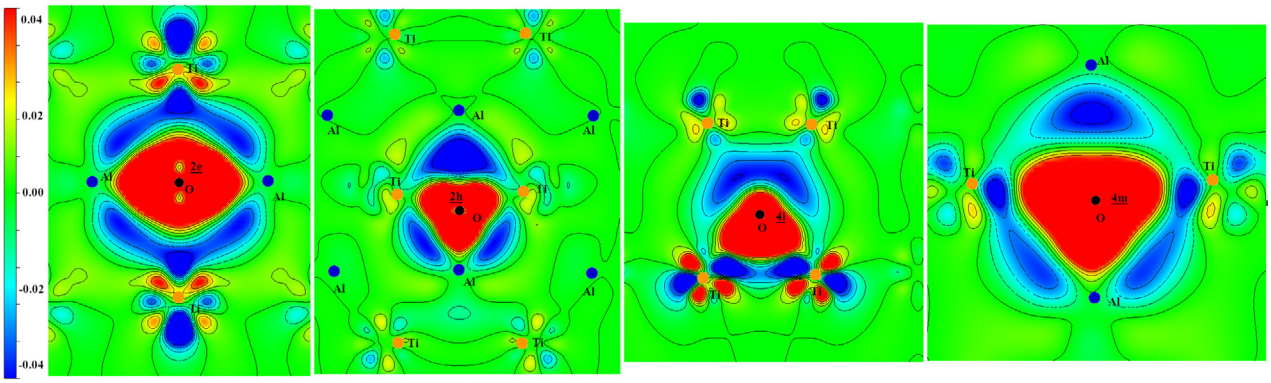

Figure 4. Charge transfer, $\Delta\rho$ (in e/$\mathring{A}^3$), when sites are filled: oxygen in *2e* (2D data displays in the [1 0 − 1] direction), *2h* ([−1 1 0]), *4i* ([−1 0 0]) and *4m* ([1 − 1 0]) sites. Al atoms are in blue, Ti atoms in orange and O in black.

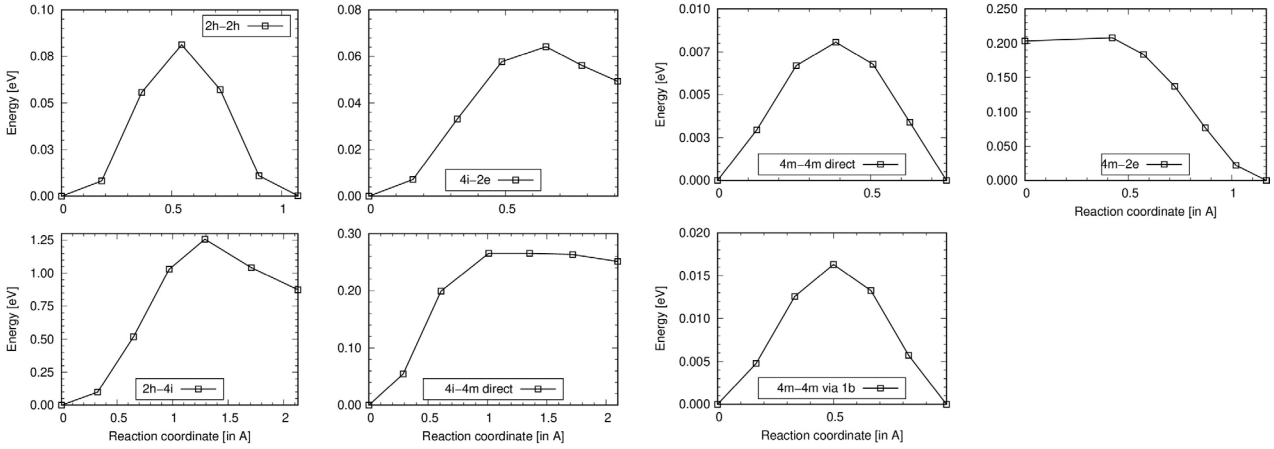

Figure 5. Plots of the energy landscape of NEB calculations for O atoms along different paths.

The maximum transfer value is located between O and Al atoms. These electrons come from Ti–Al bonds towards the O atom and reduces the stability of the bonds around the insertion sites.

In conclusion, DFT simulations shows that there is one main stable interstitial site for oxygen and when O is inserted on this stable site, interaction O–Al are minimum. In addition, insertion of O on the stable interstitial site weakness surrounding Ti–Al bonds.

Table 4. Migration energy (E_m^{ab}, in eV) of jumps from *a* to *b*.

$b \setminus a$	*2e*	*2h*	*4i*	*4m*
2e	—	—	0.07	<0.01
2h	—	0.08 [*1c*]	0.34	—
4i	0.02	1.26	—	0.02
4m	0.20	—	0.27	<0.01

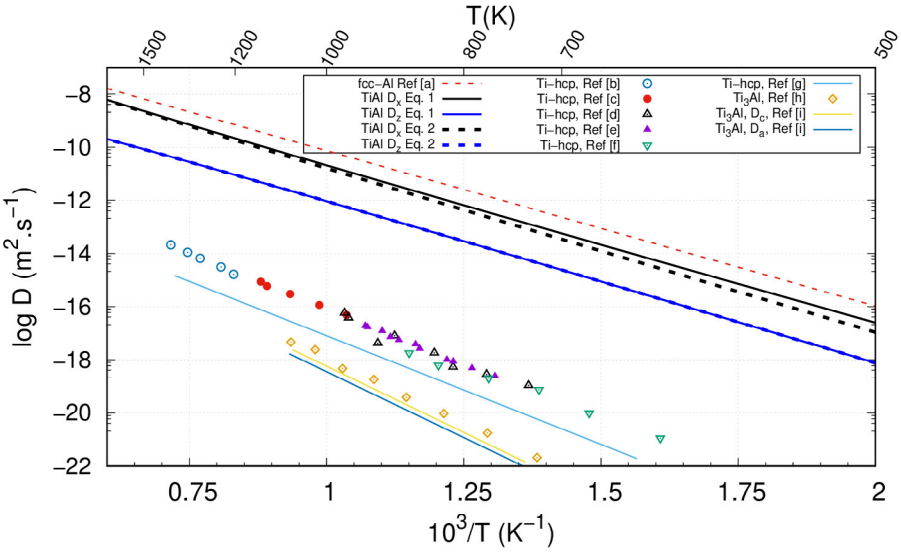

Figure 6. Diffusion coefficients of oxygen as a function of 1/T. Al: (a) = [29]; Ti-hcp: (b) = [30], (c) = [31],; (d) = [32], (e) = [33], (f) = [34], (g) = [35]; Ti_3Al: (h) = [36]; (i) = [25].

Table 5. Activation energies (E_a, in eV) and D_o (in 10^{-6} m^2 s^{-1}) obtained from an Arrhenius fit. The label † and ‡ refer to the model 1 and 2 respectively.

Direction	E_a	D_o
x, *y*	$1.197^\dagger/1.246^\ddagger$	$22.43^\dagger/30.78^\ddagger$
z	$1.189^\dagger/1.189^\ddagger$	$0.92^\dagger/0.91^\ddagger$

4. Oxygen diffusivity

The question of interest now is to determine how the O atom diffuses in the TiAl system. As seen before, O atoms can occupy many stable insertion sites, which induces many possible jumps.

To simplify, *4k* sites were omitted, because *4k* and *4m* sites are very close ($d < 0.35$ Å) and have almost the same energy. The barrier energy between both sites is therefore necessarily very low, <10 meV. Therefore, *4k* sites do not influence the diffusion coefficient. By omitting the *4k* sites, the number of jumps between *2h*, *2e*, *4m* and *4i* sites is reduced. The first jump consists of a jump between two first-nearest neighboring *2h* sites. Then, we considered two jumps to escape from a *2h* site directly to a *4i* site or to a *4m* site. Once it escaped, the O atom can then move between *2e*, *4m* and *4i* sites. The jumps between *2e- 2e* sites via *1b*, and between *1c– 1c* (or *4i– 4i*) via *2f* were omitted. As explained in the previous section, oxygen shows two-imaginary frequencies in the *2f* and *1b* sites. These configurations are second-order transition states, their jump rates are smaller (see appendix A), short-cuts are preferred. Figure 5 summarizes the energy landscapes of the jumps computed using NEB calculations. Six paths were finally considered as acceptable jumps, as depicted in figure 1. Their migration energies are summarized in table 4.

As explained above, to move from a *2h* to another *2h* site, the O atom passes through a *1c* site. The barrier is low, about 80 meV. The direct jump between *2h* and *4m* is found impossible (not represented here). Indeed, the O atom prefers to go through a *4i* site first. Most of the energy barriers are low, in the range of 0.10–0.30 eV. The limiting step is consequently the jump from a *2h* site to a *4i* site, with an energy of 1.26 eV. This significant value is the consequence of the high stability of *2h* configuration as compared to the other configurations, therefore the energy cost to leave the site is important. This site is a local 'trap' for the O atoms. These results suggest that diffusion along the *z* axis should be slower than in the $x - y$ directions, because it requires going through a *2h* site.

The macroscopic diffusion can now be computed. Due to the symmetry of the system, oxygen has two distinct diffusion coefficients, D_z and $D_{x,y}$. In first-approximation, as the residence time in the *4i*, *4m* and *4k* sites is small (low energy barriers), only the jumps between *2e* and *2h* sites were considered. The diffusion coefficients can then be expressed simply in terms of Γ_{he}, Γ_{eh}, Γ_{hh}, Γ_{ee}, the jump rates of *2h- 2e*, *2e- 2h*, *2h- 2h* and *2e- 2e* jumps, respectively, and a_o and c_o, the lattice parameters. Γ were plotted in appendix A. By applying Landman's method [28], we found:

$$D_{x,y} = \frac{a_o^2}{2} \cdot \frac{(\Gamma_{ee} + 2\Gamma_{eh})\Gamma_{he}}{\Gamma_{eh} + \Gamma_{he}} \tag{6}$$

$$D_z = c_o^2 \cdot \frac{\Gamma_{eh}\Gamma_{he}\Gamma_{hh}}{(\Gamma_{eh} + \Gamma_{he})(2\Gamma_{he} + \Gamma_{hh})} \tag{7}$$

where $a_o = 2.822$ Å and $c_o = 4.076$ Å. By combining equations (6) and (7), the degree of anisotropy of the diffusion coefficient, A_D, is given by:

$$A_D = \frac{D_z}{D_x} = \left(\frac{c_o}{a_o}\right)^2 \cdot \frac{2\,\Gamma_{eh}\Gamma_{hh}}{(\Gamma_{ee} + 2\Gamma_{eh})(2\Gamma_{he} + \Gamma_{hh})}. \tag{8}$$

A second set of equations (B.3) and (B.4), which includes *4i* sites, was also deduced, see appendix B. It will help to evaluate the accuracy of the approximations.

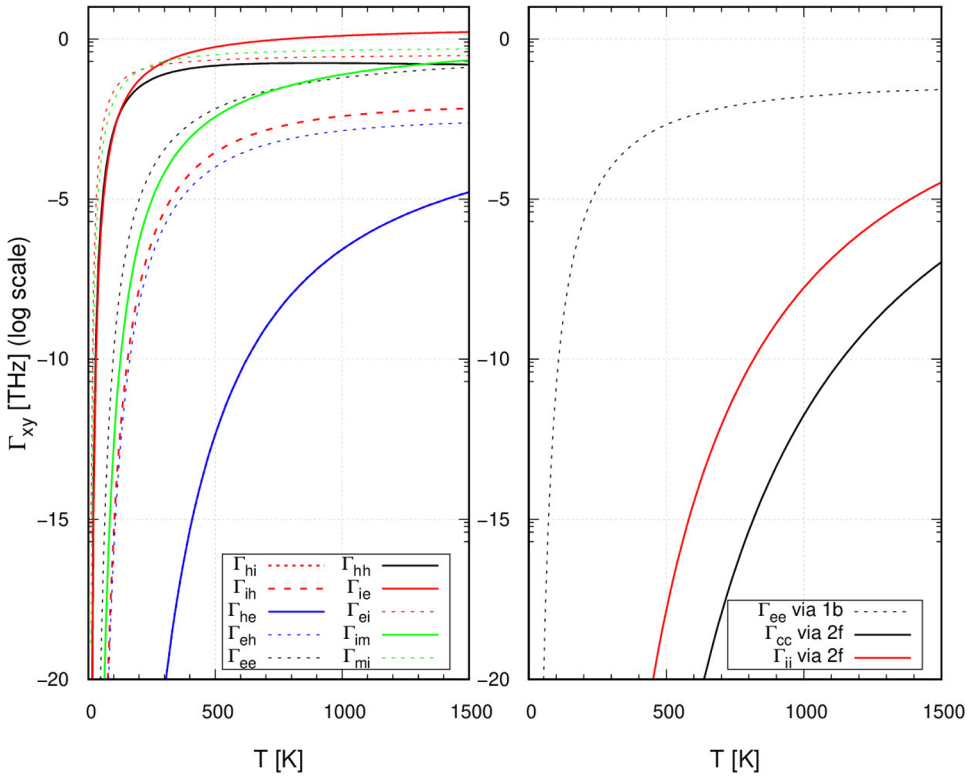

Figure A1. Attempt frequencies of all jumps as a function of T.

The diffusion coefficients, D_x and D_z, were calculated using DFT results and are depicted in figure 6. An Arrhenius fit was applied to the oxygen diffusion coefficients, $D[T] = D_o \exp(-E_a/k_B T)$, to obtain D_o and activation energies, E_a. Parameters are summarized in table 5. As is the case for hydrogen [20], the oxygen diffusion is anisotropic in the TiAl system. It is almost two orders of magnitude faster in the x-y plans than along the z direction. The slopes are quantitatively the same, only the value of D_o changes. A_D can be approximated by $A_D \propto \Gamma_{eh}/\Gamma_{ee}$ ($\Gamma_{hh} \ll \Gamma_{he}$ and $\Gamma_{ee} \ll \Gamma_{eh}$). The difference between both jumps is small, thus explaining the anisotropy.

Again, there is no experimental data to compare with the theoretical diffusion coefficients found here. Our results can be seen as the upper limit of the diffusion coefficient in the bulk. In our numerical experiments, oxygen is located in interstitial sites, i.e. the O atom is not supposed to form clusters in the metal. The oxygen therefore diffuses from one interstitial site to another, as described above, so the result presented above should be accurate. However, if O atoms form clusters with vacancies for instance, it is reasonable to assume that oxygen diffusion would be slower in the bulk. The diffusivity of O atoms should depend on the concentration of these clusters, which can therefore be considered as traps [37]. Oriani's model [38] is thus accurate enough to describe the diffusion coefficient in first approximation. However, this model still requires using ideal diffusion coefficients.

To highlight these results, the diffusion of oxygen in the TiAl- $L1_0$ system is compared with its diffusion in the Ti-hcp [32, 35], fcc-Al [29] and Ti_3Al- $D0_{19}$ [25, 36] systems, as reported in figure 6. It is obvious that oxygen diffuses faster in TiAl than in the other titanium compounds, between 3 and 6 orders of magnitude faster. By contrast, the diffusion is slightly slower than in fcc-Al [29]. Two antagonistic effects can be highlighted: the solubility is lower in TiAl than in Ti_3Al or Ti, but diffusion is much faster. In the Ti_3Al system, the stable configuration—oxygen surrounded by Ti atoms only [25]—is much more stable than the other sites that are composed of Al atoms. However, to diffuse, the O atom must necessarily pass through less stable sites, surrounded by Al atoms, so it diffuses slowly. In the case of the γ-TiAl system, results show that the most stable site is in the vicinity of an Al atom. This explains why oxygen is less stable in γ than in α_2-Ti_3Al, and consequently its lower solubility in TiAl than in Ti_3Al. However, on the other hand, the energy difference between stable sites in TiAl- $L1_0$ is smaller than in Ti_3Al- $D0_{19}$. The O diffusivity in $L1_0$ is thus faster than in $D0_{19}$.

From these results, it can be assumed that modifying the Al/Ti ratio should have an impact on the solubility and diffusion of O in the TiAl- $L1_0$ system. The chemical homogeneity of insertion sites in the TiAl system induces in smaller migration energies than in other Ti–Al alloys.

5. Conclusion

This manuscript presents a complete study of the insertion and diffusion of oxygen in TiAl- $L1_0$ system. Different stable sites were found, but one site, the *2h* site, is significantly more stable than the others. The interactions with Al atoms are stronger than with Ti atoms, and the *2h* site minimizes them. Results indicate that the preferred site (*2h*) minimizes elastic effects, but most importantly reduces the number of O–Al interactions.

A study of the trajectories at the atomic scale, by analyzing each possibility, was carried out. New explicit expressions of diffusion coefficients were given, taking into account the main configurations. Results show that, generally speaking, O atoms diffuse slowly in the TiAl- $L1_0$ system, but significantly faster than in the other Ti–Al alloys.

From these results, it can be assumed that by adjusting the Ti/Al ratio of the TiAl system, it is possible to modify oxygen solubility and diffusivity. As explained above, the O atom prefers to minimize its number of Al–O bonds. It can therefore be expected that increasing (decreasing) the Al content should induce a decrease (resp. increase) in the amount of true ' *2h*' sites in the metal. The oxygen concentration should thus decrease (resp. increase). However, this Al increase (decrease) should also induce an increase (resp. decrease) in oxygen diffusivity, due to fewer (resp. more) *2h* sites/traps. Nevertheless, these antagonistic effects are in fact difficult to separate. The true important quantity is indeed the flux of matter, so more exhaustive models are required to further evaluate the penetration of oxygen.

We thus reported here a number of data useful in the build of empirical potentials for the Ti–Al–O system.

Acknowledgments

This work was performed using HPC resources from CALMIP (Grant 2019-p0749 and p0912).

Appendix A. Attempt jumps

The attempt frequencies for all jumps studied were drawn in figure A1. They were computed using migration energies summarized in table 4 and Helmholtz vibration energies. The jump probability through second-order transition states is systematically low, even in the case of Γ_{ee} via the *1b* site, where the migration energy is low. This is an argument in favor of not taking them into account in the process at the atomic level.

Appendix B. Multi-states model

The same method as presented in [20] was used to derive diffusion equations. In the first set of equations, the number of jumps were reduced, to simplify the atomistic process. Only *2h* and *2e* sites were retained. The O atom can jump between *2h* sites. It can also jump from a *2h* to a *2e* sites directly, the transition state considered was that of the jump between *2h*-*4i*. In *4i*, the O atom is considered to jump instantaneously in a *2e* site. Then in *2e*, the O atom can move through another *2e* site via the *4m* site. Four quantities characterize the diffusion coefficients: Γ_{ee}, Γ_{he}, Γ_{he} and Γ_{ee}. The diffusion coefficients are therefore equal to:

$$D_{x,y} = \frac{a_o^2}{2} \cdot \frac{(\Gamma_{ee} + 2\Gamma_{eh})\Gamma_{he}}{\Gamma_{eh} + \Gamma_{he}} \tag{B.1}$$

Table B1. Migration energies (E_m^{ab}, in eV) of jumps from *a* to *b* for the second model.

$b \setminus a$	*2e*	*2h*
2e	0.20 (via *4m*)	1.26 (via *4i*)
2h	0.34 (via *4i*)	0.08

Table B2. Migration energies (E_m^{ab}, in eV) of jumps from *b* to *a* for the second model.

$b \setminus a$	*2e*	*2h*	*4i*
2e	0.20 (via *4k*)	—	0.07
2h	—	0.08	0.34
4i	0.20	1.26	—

$$D_z = c_o^2 \cdot \frac{\Gamma_{eh}\Gamma_{he}\Gamma_{hh}}{(\Gamma_{eh} + \Gamma_{he})(2\Gamma_{he} + \Gamma_{hh})} \tag{B.2}$$

where $a_o = 2.822$ Å and $c_o = 4.076$ Å. Migration energies are listed in table B1.

To improve this model, the *4i* sites were included. Equations become:

$$\begin{aligned} D_{x,y} = \frac{a_o^2}{2}\Gamma_{hi}(&\Gamma_{ee}\Gamma_{hh}\Gamma_{ie}^2 + 2\,\Gamma_{ee}\Gamma_{hi}\Gamma_{ie}^2 + 2\,\Gamma_{ee}\Gamma_{hh}\Gamma_{ie}\Gamma_{ih} \\ &+\Gamma_{ei}\Gamma_{hh}\Gamma_{ie}\Gamma_{ih} + 4\,\Gamma_{ee}\Gamma_{hi}\Gamma_{ie}\Gamma_{ih} + 2\,\Gamma_{ei}\Gamma_{hi}\Gamma_{ie}\Gamma_{ih} \\ &+2\,\Gamma_{ei}\Gamma_{hh}\Gamma_{ih}^2 + 6\,\Gamma_{ei}\Gamma_{hi}\Gamma_{ih}^2) \\ /\,((2\,\Gamma_{ei}\Gamma_{hi} + \Gamma_{hi}\Gamma_{ie} + \Gamma_{ei}\Gamma_{ih})&(\Gamma_{hh} + 2\,\Gamma_{hi})(\Gamma_{ie} + 2\,\Gamma_{ih})) \end{aligned} \tag{B.3}$$

and

$$D_z = c_o^2 \frac{\Gamma_{ei}\Gamma_{hh}\Gamma_{hi}\Gamma_{ih}}{(2\,\Gamma_{ei}\Gamma_{hi} + \Gamma_{hi}\Gamma_{ie} + \Gamma_{ei}\Gamma_{ih})(\Gamma_{hh} + 2\,\Gamma_{hi})}. \tag{B.4}$$

The parameters for this model are given in table B2.

ORCID iDs

Damien Connétable https://orcid.org/0000-0003-3642-780X

References

[1] Kothari K, Radhakrishnan R and Wereley N 2012 Advances in gamma titanium aluminides and their manufacturing techniques *Prog. Aerosp. Sci.* **55** 1–16
[2] Kim Y-W 1989 Intermetallic alloys based on gamma titanium aluminide *J. Miner.* **41** 24–30
[3] Kim Y-W and Dimiduk D M 1991 Progress in the understanding of gamma titanium aluminides *J. Miner.* **43** 40–7
[4] Rahmel M S A and Quadakkers W J 1995 Fundamentals of tial oxidation—a critical review *Mater. Corros.* **46** 271–85
[5] Małecka J 2019 Transformation and precipitation processes in a metal substrate of oxidized tial-based alloys *Oxid. Met.* **91** 365–80
[6] Appel F, Paul J D H and Oehring M 2011 *Gamma Titanium Aluminide Alloys: Science and Technology* (New York: Wiley)

[7] Zghal S, Menand A and Couret A 1998 Pinning points anchoring ordinary and shockley dislocations in tial alloys *Acta Mater.* **46** 5899–905

[8] Kad B K and Fraser H L 1994 Effects of oxygen on the deformation behaviour in single-phase γ-tial alloys *Phil. Mag. Lett.* **70** 211–20

[9] Kawabata T, Abumiya T and Izumi O 1992 Effect of oxygen addition on mechanical properties of tial at 293–1273 k *Acta Metall. Mater.* **40** 2557–67

[10] Menand A, Huguet A and Nérac-Partaix A 1996 Interstitial solubility in γ and α_2 phases of tial-based alloys *Acta Mater.* **44** 4729–37

[11] Barouh C, Schuler T, Fu C-C and Nastar M 2014 Interaction between vacancies and interstitial solutes (c, n, and o) in α-fe: from electronic structure to thermodynamics *Phys. Rev.* B **90** 054112

[12] Connétable D, David M, Prillieux A, Young D and Monceau D 2017 Impact of the clusterization on the solubility of oxygen and vacancy concentration in nickel: a multi-scale approach *J. Alloys Compd.* **708** 1063–72

[13] Kresse G and Hafner J 1993 *Ab initio* molecular dynamics for liquid metals *Phys. Rev.* B **47** 558–61

[14] Kresse G and Joubert D 1999 From ultrasoft pseudopotentials to the projector augmented-wave method *Phys. Rev.* B **59** 1758–75

[15] Perdew J P, Burke K and Ernzerhof M 1996 Generalized gradient approximation made simple *Phys. Rev. Lett.* **77** 3865–8

[16] Monkhorst H J and Pack J D 1976 Special points for brillouin-zone integrations *Phys. Rev.* B **13** 5188–92

[17] Henkelman G, Uberuaga B P and Jónsson H 2000 A climbing image nudged elastic band method for finding saddle points and minimum energy paths *J. Chem. Phys.* **113** 9901–4

[18] Eyring H 1935 The activated complex in chemical reactions *J. Chem. Phys.* **3** 107–15

[19] Togo A, Oba F and Tanaka I 2008 First-principles calculations of the ferroelastic transition between rutile-type and $cacl_2$-type SiO_2 at high pressures *Phys. Rev.* B **78** 134106

[20] Connétable D 2019 Theoretical study on hydrogen solubility and diffusivity in the γ-tial $L1_0$ structure *Int. J. Hydrog. Energy* **44** 12215–27

[21] Aroyo M I, Perez-Mato J M and Capillas C 2009 Bilbao crystallographic server: I. databases and crystallographic computing programs *Z. Kristallogr.* **221** 15–27

[22] Connétable D and David M 2019 Diffusion of interstitial species (h and o atoms) in fcc systems (Al, Cu, Co, Ni and pd): Contribution of first and second order transition states *J. Alloys Compd.* **772** 280–7

[23] Bakulin A V, Kulkova S E, Hu Q M and Yang R 2015 Theoretical study of oxygen sorption and diffusion in the volume and on the surface of a γ-tial alloy *J. Exp. Theor. Phys.* **120** 257–67

[24] Wei Y, Zhou H-B, Zhang Y, Lu G-H and Xu H 2011 Effects of o in a binary-phase TiAl–Ti3Al alloy: from site occupancy to interfacial energetics *J. Phys.: Condens. Matter* **23** 225504

[25] Bakulin A V, Latyshev A M and Kulkova S E 2017 Absorption and diffusion of oxygen in the Ti3Al alloy *J. Exp. Theor. Phys.* **125** 138–47

[26] Varvenne C, Bruneval F, Marinica M-C and Clouet E 2013 Point defect modeling in materials: coupling *ab initio* and elasticity approaches *Phys. Rev.* B **88** 134102

[27] Henkelman G, Arnaldsson A and Jónsson H 2006 A fast and robust algorithm for bader decomposition of charge density *Comput. Mater. Sci.* **36** 354–60

[28] Landman U and Shlesinger M F 1979 Stochastic theory of multistate diffusion in perfect and defective systems. II. Case studies *Phys. Rev.* B **19** 6220–37

[29] David M and Connétable D 2017 Diffusion of interstitials in metallic systems, illustration of a complex study case: aluminum *J. Phys.: Condens. Matter* **29** 455703

[30] Rosa C J 1970 Oxygen diffusion in alpha and beta titanium in the temperature range of 932 °C–1142 °C *Metall. Trans.* **1** 2517–22

[31] Dechamps M and Lehr P 1977 Sur l'oxydation du titane α en atmosphère d'oxygène: Rôle de la couche oxydée et mécanisme d'oxydation *J. Less Common Met.* **56** 193–207

[32] David D, Beranger G and Garcia E 1983 A study of the diffusion of oxygen in α-titanium oxidized in the temperature range 460 °C–700 °C *J. Electrochem. Soc.* **130** 1423–6

[33] Vykhodets V, Klotsman S, Kurennykh T, Levin A and Pavlov V 1989 Oxygen diffusion in α-Ti *Fiz. Met. Met.* **68** 723–7

[34] Bregolin F, Behar M and Dyment F 2007 Diffusion study of 18° implanted into α-Ti using the nuclear resonance technique *Appl. Phys.* A **86** 481–4

[35] Wu H H and Trinkle D R 2011 Direct diffusion through interpenetrating networks: oxygen in titanium *Phys. Rev. Lett.* **107** 045504

[36] Koizumi Y, Yoshiya M, Sugihara A and Minamino Y 2011 Effect of impurity atoms on alpha-2/gamma lamellar interfacial misfit in Ti–Al alloy: a systematic first principles study *Phil. Mag.* **91** 3685–704

[37] Hodille E, Ferro Y, Fernandez N, Becquart C, Angot T, Layet J-M, Bisson R and Grisolia C 2016 Study of hydrogen isotopes behavior in tungsten by a multi trapping macroscopic rate equation model *Phys. Scr.* **2016** 014011

[38] Oriani R A 1970 The diffusion and trapping of hydrogen in steel *Acta Met.* **18** 147–57